Where Do the Ions Reside in a Highly Charged Droplet? Effect of the Ion Spatial Distribution on the Droplet Electric Field

Victor Kwan,[†] Anatoly Malevanets,[‡] and Styliani Consta[*,†]

†*Department of Chemistry, The University of Western Ontario, London, Ontario, Canada N6A 5B7*

‡*Department of Electrical and Computer Engineering, The University of Western Ontario, London N6A 5B9, Ontario, Canada*

E-mail: sconstas@uwo.ca

Abstract

Droplets in atmospheric and electrosprayed aerosols carry more often than not, a multitude of ions. We address the question of the spatial distribution of a collection of ions in charged aqueous droplets with linear dimensions in the nanometer range (the diameter is ≈5 nm and ≈8.5 nm in the simulated drops). In the study we use atomistic modeling and analytical theory. The charge carriers are solely Na^+ ions and a mixture of Na^+ ions and a macroion with high degree of hydrophilicity. We find that the Na^+ ion density is higher near the droplet surface at the place where the water density is still high, and it is non-negligible in the interior of the droplet. The simulation results are supported by a general analytical theory that takes into account a fluctuating droplet interface, a Debye screening of the charges and the finite size of a solvated ion. The fact that the analytical theory predicts the general features of the ion distribution may suggest that this distribution is largely due to fundamental effects included in the model. We compute the electric potential and the electric field near the droplet surface using a multipole expansion. We establish that an equipotential surface is found in the interior near the droplet surface. We attribute the shift of the molecular surface used in the Rayleigh limit toward the interior of the droplet to the finite size of the solvated ions. In the presence of a highly charged peptide we find that the peptide is more likely to be situated in the interior of the droplet while the simple ions are found near the droplet surface. Density calculations reveal that it is likely for macroions with high charge, thus with high degree of hydrophilicity, to be found near the droplet surface. In relation to electrospray mass spectrometry experiments the presence of macroions near the surface may affect their charging mechanism and release from a droplet. The study sheds light into a long-standing debate regarding the spatial distribution of multiple ions in a droplet and provides insight into droplet chemistry.

Introduction

Charged droplets are ubiquitous in atmospheric and man-made aerosols. More often than not, these droplets comprise several ions instead of a single ion. Thus far, there have been many studies on the location of a single ion in clusters with dimensions up to a few nanometers in diameter.[1–12] Differently, the study of the structure of charged clusters with multiple ions has been initiated but it is still incomplete.[13–22] In this article we investigate the spatial distribution of ions in multiply charged mesoscopic clusters and the structure that the ions induce in

the solvent. The mesoscopic clusters are often called nano-drops.

The multiply charged droplets play a central role in many applications. Charged droplets are the constituents of man-made aerosols that are generated by a variety of spraying methods.[23] In particular, droplets generated by electrospraying have found numerous applications, among which are in the production of nanoparticles,[24] in achieving acceleration of several reactions relative to their bulk analogues,[25–29] and in ionization methods coupled to mass spectrometry.[30] In many of these applications the reaction mechanisms are unknown. For instance, it is still an open question why certain reactions are accelerated and others are decelerated relative to their bulk analogues when they take place in an electrosprayed droplet.[25–29] The spatial distribution (concentration) of the ions may provide a clue as to where ion and charge transfer reactions may take place and thus, assist in unraveling the reaction mechanisms. The reactivity within a charged droplet is also of central interest in native mass spectrometry (MS) where often droplet-based ionization techniques[31–34] such as electrospray ionization (ESI) are used.[30,35–39] In ESI-MS depending on the purpose of the designed experiment the initial droplet diameter may be of a few microns or of a few hundreds of nanometers down to a few tens of nanometers.[40] In various ESI-MS experiments a droplet of certain size will differ in composition, and temperature due to differences in the composition of the parent bulk solution, history to reach a certain size and the experimental set-up. However, charged droplets of a specific size and of the same solvent regardless of the spraying conditions have a common feature: they sustain approximately the same amount of maximal charge.[19,41] We will explain in the next paragraphs the origin of the common maximal charge.

A fundamental question in the study of charged droplets is on the conditions for stability. Even though in this article we do not analyze the droplet stability,[41–44] it is important to discuss the maximal amount of charge a droplet may sustain in order to justify the amount of charge in the studied droplets. The fundamental theory for the stability of a charged conducting droplet was developed by Lord Rayleigh.[41–44] The strength of the Rayleigh theory lies on the fact that the droplet shape fluctuations are taken into account in the model while the study of the stability of a non-fluctuating spherical droplet is a much simpler problem.

In the Rayleigh model the energy of a conducting droplet is written as the sum of surface energy ($E_{\rm surf}$) and electrostatic energy ($E_{\rm el}$)

$$E = E_{\rm el} + E_{\rm surf} = \gamma A + \frac{1}{2} QV \qquad (1)$$

where Q, γ, A, V are the droplet charge, the surface tension, the surface area and the electrostatic potential, respectively. Linear stability analysis provides the critical charge-squared-to-volume ratio below which a conducting droplet is stable. This ratio is a dimensionless parameter, which is called the fissility parameter (X), and it is defined as

$$X = \frac{Q^2}{64\pi^2 \gamma \varepsilon_0 R^3} \qquad (2)$$

where ε_0 and R are the permittivity of vacuum and the radius of the droplet, respectively. The other symbols have the same meaning as in Eq. 1. When X is less than unity, the system is stable. At $X = 1$ the droplet is at the Rayleigh limit, and when $X > 1$ the system is unstable. In terms of forces, a charged droplet is unstable when the electrostatic forces among the ions of the same sign overcome the surface tension force. Rayleigh's model has been extended to dielectric droplets.[45] The extension provides a more general theory, out of which the stability condition for conducting droplets emerges when the droplet dielectric constant goes to infinity. Because of this universal stability condition, regardless of the method of production of the highly charged droplets and their history to reach a certain size, all droplets of the same size and solvent will sustain approximately the same amount of maximal charge.[19] Many experiments and computational studies have confirmed the validity of the Rayleigh limit.[13,14,21,45,46] The nanodrops we simulate are

found at $X \approx 0.9$ (Eq. 2) in order for them to be stable and to be close to the charge state of electrosprayed droplets.[47]

In this article we examine the spatial distribution of ions in nanoscopic aqueous drops, by using atomistic modeling and an analytical theory. We study two cases of charge distributions: (a) The charge carriers are simple ions. We have selected to use Na^+ ions to demonstrate the effects. The insight we obtain from the study of the Na^+ ions is general and applicable to all the other mono-monovalent ions. (b) The charge carriers are simple ions and a macroion. Na^+ ions and a charged polyhistidine are used as an example and once more the findings have general applicability to similar systems. To our knowledge, the size of droplets under investigation with an approximate diameter of 5 nm and 8.5 nm are possibly the largest that have been reported. The analytical theory combines the charge distribution in a fluctuating interface, an effective screening length (we call it a Debye length) estimated by the solution of the non-linear Poisson-Boltzmann equation[48] and the finite size of a solvated ion. Comparison of the analytical theory with the simulation data, shows that all the features of the ion spatial distribution in the charged droplets can be captured.

In our studies we find a different single ion and multiple ion spatial distributions from previous works.[15,16] We emphasize the significance of thorough equilibration in order to obtain converging spatial distributions of ions. We discuss the origin of the differences in the analysis of the data.

In the charged droplets we computed the electric potential and the electric field using a multipole expansion. The values of the electric potential were interpolated after regularization onto the molecular surface of a drop. The Rayleigh limit ($X = 1$ in Eq. 2) assumes that the potential in a droplet is constant on the surface. In the aqueous droplets with Na^+ ions we established the existence of an equipotential surface at 1.7 Å inside the drop, which is not where the Na^+ ions are located. We may consider a shift of the molecular surface that enters the Rayleigh limit toward the interior of the droplet due to the finite size of the solvated ions.

In the aqueous droplets that contain single ions and a macroion, we show that, occasionally, macromolecules with high charge and, therefore, with high degree of hydrophilicity are found near the droplet surface. Their transfer to the surface may be associated with droplet shape fluctuations between prolate and spherical shapes. This finding is to complement the view that macromolecules with high degree of hydrophobicity and even macromolecules classified as hydrophilic such as poly(ethylene glycol) (PEG)[49,50] can expose part of their structure in the droplet-vacuo (or vapor) interface. The spatial distribution of the macroions and simple ions may provide insight into the charging mechanisms of the macroions that are detected in ESI-MS experiments. In order to characterize the droplet structure we also examine the water dipole orientations due to the internal electric field.

Our study will start with the discussion of structural features of pristine aqueous droplets in order to use them as reference systems. Then, we will examine the droplet structure in the presence of single ions and macroions. In order to perform a systematic study we have not considered the effect of counterions. Some aspects of the effect of counterions have been discussed in our previous articles[19] and we follow-up on this study.

Systems and Simulation Methods

We performed equilibrium molecular dynamics (MD) simulations of pristine and charged aqueous droplets with sodium ions and peptides. The simulations were performed by using the software NAMD version 2.12.[51] Newton's equation of motion for each atomic site was integrated using the velocity-Verlet algorithm with a time step of 1.0 fs. The trajectories were analyzed using VMD 1.9.2.[52] The peptides were modeled with CHARMM forcefield, and the water was modeled with the TIP3P (transferable intermolecular potential with 3 points)-

CHARMM.

All the forces were computed directly without any cut-offs. Equilibrium simulations in NAMD were set by placing the droplet in a spherical cavity of radius 20.0 nm by using spherical boundary condition. The cavity was sufficiently large to accommodate the shape fluctuations of the droplet. The droplet will eventually reach vapor pressure equilibrium. The systems were thermalized with Langevin thermostat with the damping coefficient set to 1/ps. The Rayleigh limit of the droplet (Eq. 2) was calculated with the surface tension values of the water model used at the simulation temperature.[53]

Pristine and sodiated aqueous droplets

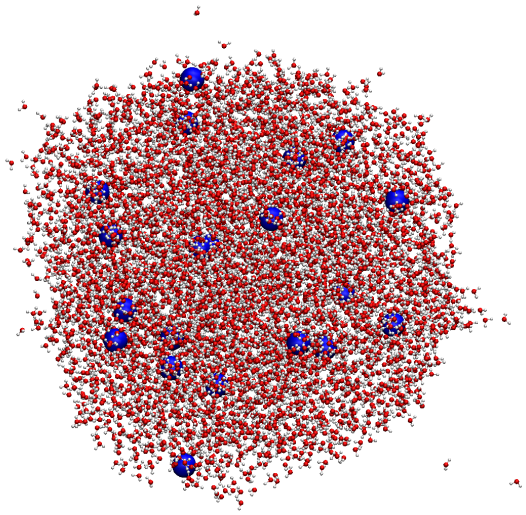

Figure 1: Typical snapshot of a droplets comprised 6000 TIP3P molecules (oxygen sites are represented by red spheres and hydrogen sites by white) and 20 Na^+ ions (represented by blue spheres). The Na^+ ions have been enlarged for clarity.

We performed equilibrium MD simulations of droplets comprised (a) $\approx$ 1000 H_2O molecules, which correspond to a diameter of $\approx$ 4 nm and (b) $\approx$ 6000 H_2O molecules, which correspond to a diameter of $\approx$ 8.5 nm. The droplet compositions are: (a) with water only; (b) water and Na^+ ions at $X = 0.9$ and (c) water with a single Na^+ ion. Specifically, the larger droplets (when equilibrium between the vapor and the droplet has been established) are composed on average of 6130 and 5990 H_2O molecules at 300 K and 350 K, respectively. The sodiated 6000-H_2O droplet has 20 Na^+ ions. At 350 K up to two Na^+ ions have escaped from the droplet and remain in the cavity. A typical snapshot of the 6000-H_2O droplet with 20 Na^+ ions is shown in Fig. 1.

The smaller H_2O droplet comprise on average 990 and 890 H_2O molecules at 300 K and 350 K, respectively. These droplets are charged with 8 Na^+ ions. The production runs for the $\approx$ 1000 H_2O-8 Na^+ ions systems were for 60 ns and for $\approx$ 6000 H_2O-20 Na^+ ions 24 ns at both $T = 300$ K and 350 K. Simulations of 60 ns were also performed for the $\approx$ 1000 H_2O-molecule droplets with a single Na^+.

Polyhistidine in a conducting aqueous droplet

We performed equilibrium MD simulations of droplets comprised initially 6057 H_2O, 10 Na^+ ions and a completely charged polyhistidine of 10 residues (His_{10}^{10+}). Since the 6057 H_2O droplet is placed in a cavity, a portion of the H_2O will evaporate, leaving a droplet of $\approx$ 5883 H_2O molecules. The production run was for 50 ns and the temperature 350 K.

To compare the effect of the length of the peptide on the ion spatial distribution, we also performed equilibrium MD simulations on a 20-histidine chain (His_{20}^{10+}), which consisted of alternating protonated and unprotonated histidine residues. The simulations were performed under the same conditions as those of the His_{10}^{10+} system.

Results and Discussion

Structure of pristine aqueous droplets

The structure of pristine water droplets up to 512 H_2O molecules for the five-site ST2 model, the four-site TIP4P model and the SPC/E (extended simple point charge) and that of 1000 H_2O molecules for certain water models has

been examined in detail by Zakharov and coworkers.[54,55] The authors examined the sensitivity of the surface potential and surface tension on ST2, TIP4P, SPC/E water models. In our article we are mainly interested in the structure of the charged droplets, but we shall also discuss some of the characteristics of the pristine aqueous droplets modeled by TIP3P for the sake of completeness. The bulk density of the TIP3P water model at 25° C and pressure 1.0 atm has been calculated[56,57] to be 1.002 ± 0.001 g/cm^3 but also values of 0.998 g/cm^2 have been reported depending on subtle details of the parametrization.[58]

Figure 2 (a) shows the density of the TIP3P H_2O molecules as a function of the distance (r) from the droplet center of mass (COM). The droplets comprised ≈ 1000 and ≈ 6000 TIP3P-H_2O molecules are found at $T = 300$ K and $T = 350$ K. Figure 2 (b) shows in colored shells the distances of the water molecules from the COM of a 6000-H_2O droplet. The raw data of the histograms used for Figure 2 (a) are shown in Fig. S1 in the supplementary material. The water density profile (DP) shows an almost constant value up to 12.0 Å and 23.2 Å for the 1000 and 6000 H_2O-molecule droplet, respectively. At $T = 300$ K the value of the density in the core of the droplet is higher than that of the corresponding bulk solvent. As expected at 350 K, the density is lower overall than that at 300 K. At 300 K, the decrease in density is initially smooth and it undergoes a faster decrease at $r \approx 15.9$ Å and $r \approx 31.2$ Å for the 1000 and 6000 H_2O-molecule droplet, respectively. The droplet has a rough surface. In the 6000-H_2O-molecule droplet, an obvious surface roughness starts in the grey shell as shown in Fig. 2 (b). The location of the surface in a droplet has been discussed thoroughly in many surface tension studies of curved surfaces.[53,59–66] Here, we do not address the location of the surface because we think that it is not relevant to the properties we examine. In a forthcoming article we have examined the location of the surface in relation to the surface tension of highly charged droplets.

The density profiles of the pristine water droplets can be compared with those shown

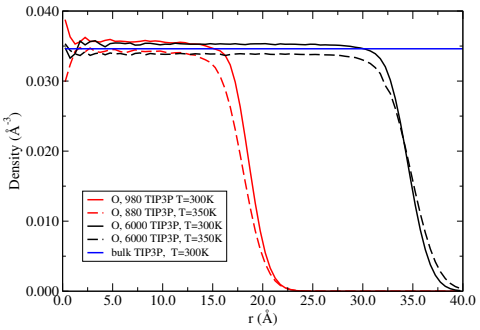

(a)

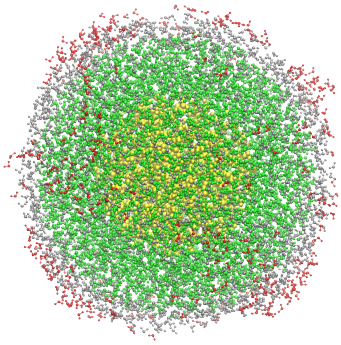

(b)

Figure 2: (a) Density of oxygen sites as a function of the distance (r) from the droplet center of mass (COM). The droplets comprised approximately 1000 and 6000 TIP3P H_2O molecules in equilibrium with its vapor at $T = 300$ K (solid lines) and $T = 350$ K (long dashed lines). The zero of the x-axis is at the droplet center of mass (COM) and the density plot starts from the center of the histogram bin, which is at 0.25 Å. The bulk density of TIP3P,[56,57] which is 0.03461 $Å^{-3}$ at $T = 300$ K and pressure 1 atm is shown by the blue line. For the histograms, we used 2×10^4 configurations each collected every 0.2 ps and a bin size is 0.5 Å. Testing of smaller bin size showed the same features in the profiles. (b) Colored shells around the 6000-TIP3P droplet COM: yellow colored 0 Å $< r <$ 17.0 Å, green colored 17.0 Å $< r <$ 30.0 Å, grey colored 30.0 Å $< r <$ 34.0 Å, red colored $r >$ 34.0 Å.

in Fig. 1 in Zakharov et al.[54,55] Calculations of Zakharov et al.[54,55] for clusters of 512 H_2O

molecules show that the clusters at $T = 300$ K modeled by TIP4P and SPC/E have a core density very close to the bulk, but that modeled by ST2 have a higher core density than that of the bulk.

We have found that the hydrogen (H) and oxygen (O) profiles almost overlay (for clarity we do not show the hydrogen profiles). We note that there is an inversion in the order of the O and H-DP as has been found by Zakharov et al.[54,55] For the 6000-H_2O droplet we found that for $r < 35.35 \pm 0.5$ Å the O-DP shows a slightly higher probability density than the H-DP. The order is inverted for $r > 35.35 \pm 0.5$ Å. The change in the order of the profiles occurs smoothly. Because of this inversion, Zakharov et al.[54,55] consider that there is an electric double layer in the surface of water clusters.

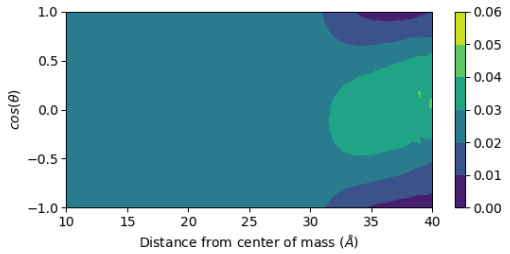

Figure 3: Contour map of $\cos(\theta)$ throughout consecutive spherical shells with center at the droplet COM for pristine aqueous droplets comprised ≈ 6000 TIP3P molecules at $T = 300$ K. The droplet configurations are the same as those used in Fig. 2. The bin size in $\cos(\theta)$ is 0.05 and in distance 0.5 Å.

In order to examine the orientation of the electric dipoles within the droplet, we compute the distribution of $\cos(\theta)$, where θ is the angle between the H_2O dipole moment (directed from the oxygen site to the center of the line that connects the two hydrogen sites) and the vector that points from the droplet center of mass (COM) to the oxygen site of a water molecule. Both the 1000 and 6000 H_2O-molecule droplet show the same features in the angle distribution. Here we describe only that of the 6000 H_2O-molecule droplet and that of the 1000 H_2O-molecule droplet is shown in Fig. S2 in the supplementary material. Figure 3 shows in a contour plot the $\cos(\theta)$ distribution for a droplet of 6000 TIP3P molecules at $T = 300$ K. The $\cos(\theta)$ distributions within representative spherical shells (with center at the droplet COM) for 1000 and 6000-H_2O-molecule droplet are shown in Figs. S3 and S4 in the supplementary material. At $r < 28$ Å the

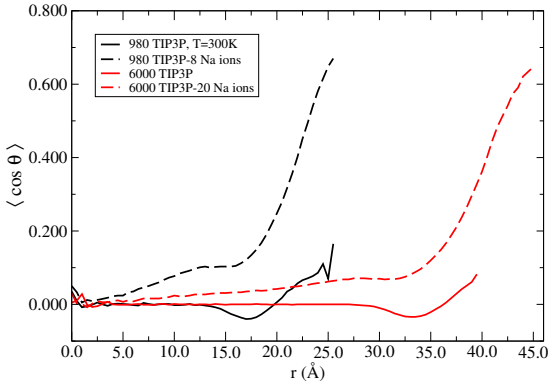

Figure 4: $\langle\cos(\theta)\rangle$ as a function of the distance (r) from the droplet COM for pristine and sodiated aqueous droplets, comprised 980 and 6000 TIP3P H_2O molecules at $T = 300$ K.

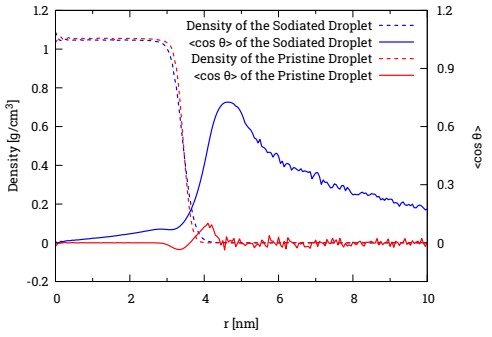

(a)

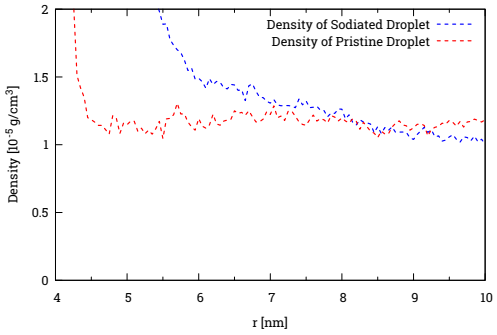

(b)

Figure 5: (a) $\langle\cos(\theta)\rangle$ as a function of r for a pristine and sodiated 6000-TIP3P droplet and vapor in the cavity at $T = 300$ K. The density profiles of water are shown. (b) Magnification of the TIP3P density decay at $r > 4$ nm of (b).

$\cos(\theta)$ distribution is uniform. The same feature has been found in other works[16,54,55] but for droplets of different size from that that we study. Thus, regardless of the size of the droplet and the water model this feature is robust. At 28 Å$< r <$ 35 Å the $\cos(\theta)$ distribution is an inverted parabola (shown in Figs. S3 and S4 in the supplementary material), with a flat maximum in range $-0.25 - 0$. In approximately the same range of 28.0 Å$< r <$32.0 Å the raw data of the oxygen population is at its maximum (shown in Fig. S1 in the supplementary material). For $r >$ 32.0 Å the oxygen population decreases (Fig. S1 in the supplementary material) while the volume increases, which indicates a considerable decrease in the droplet density. At 35 Å$< r <$37 Å the $\cos(\theta)$ distribution in symmetric with respect to zero. At $r >$37 Å the $\cos(\theta)$ distribution shows a broad maximum in the range $0 - 0.25$. In the same distance ($r \approx$ 38.0 Å), the oxygen population decreases by an order of magnitude relative to that in the range 28.0 Å$< r <$32.0 Å. It is noted that in the non-uniform angle distribution the populations of $\cos(\theta) = \pm 1.0$ (angles of 0° and 180°) are one third to one fourth of those at the maximum. Thus, parallel and anti-parallel orientations of the dipoles with $\vec{r}$ are frequently encountered and with a modestly higher frequency of the anti-parallel orientation at a certain *dr* interval. The same features as for 300 K are also observed at temperature 350 K, however at 350 K the distribution is broader (see Fig. S3 and S4 in the supplementary material). At $T = 350$ K the shift from negative to positive $\cos(\theta)$ values is also observed as one moves from the inner to the outer solvent shells. Our results are consistent with those of Zakharov et al.[54,55] regarding the negative shift of the $\cos(\theta)$ distribution that we find in the inner water layers. Zakharov et al.[54,55] find a 90° angle in the outer layers. In the range 35.0 Å$< r <$37.0 Å, which is the red shell in Fig. 2 (b), we find that the $\cos(\theta)$ distribution is symmetric with respect to 0.0 (as shown in Fig. S4 (e) in the supplementary material). This distribution leads to $\langle\cos(\theta)\rangle = 0$ (where $\langle\cdots\rangle$ denotes average). The $\cos(\theta)$ distribution has its maximum at 0.0 (which corresponds to 90°) but the majority of the dipoles deviate from the 90° angle. The red shell is characterized by roughness, thus the 90° angle is not on a smooth surface. In the farthest outer layers, where the density is very low, we see a positive shift in the $\cos(\theta)$ distribution.

Figure 4 shows the $\langle\cos(\theta)\rangle$ as a function of r for the pristine and charged droplets at $T = 300$ K. The collection of plots for neutral and charged droplets allows for a direct comparison. Fig. 5 (a) shows that the surrounding vapor is polarized around the charge droplet and that the density of charged droplet surface is higher than that of the neutral. Fig. 5 (b) shows that in longer distance from the droplet COM the density of the vapor surrounding the neutral droplet is constant but that of the charged droplet decays. The vapor distribution around the droplet is determined by the electric field in the exterior of the droplet.

The overall picture that arises from our simulations is that at $r = 33.0 \pm 0.5$ Å, which is before a considerable decrease in the water density takes place, there is a negative shift in the $\cos(\theta)$ distribution. In the range of 35.0 Å$< r <$37.0 Å, which is the region of rough surface with low density, the $\cos(\theta)$ distribution is symmetric with respect to zero, thus, $\langle\cos(\theta)\rangle = 0$. In this shell, the majority of dipoles have an angle close to 90°, with equal probability of positive and negative deviations from the 90°.

Conducting droplets with simple ions

Figure 6 (a) shows the DP of the oxygen (O) sites of TIP3P (H_2O) molecules and the concentration profile (CP) of Na^+ ions in a droplet comprised 6130 H_2O molecules and 20 Na^+ ions at $T = 300$ K. The O-DPs and Na^+-CPs of 1000 H_2O (at $T = 300$ K and 350 K) and of 5990 H_2O-molecule droplets at $T = 350$ K are shown in Fig. S5 in the supplementary material. Figure 6 (b) shows colored aqueous shells in order to relate their location to the O-DP shown in Fig. 6 (a).

Figure 6 (a) shows that the O-DP starts to decrease at 27 Å $< r <$ 28.0 Å. As expected, the H-DP (not shown) follows very closely that

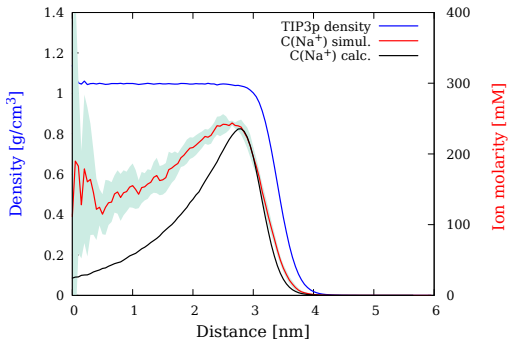

(a)

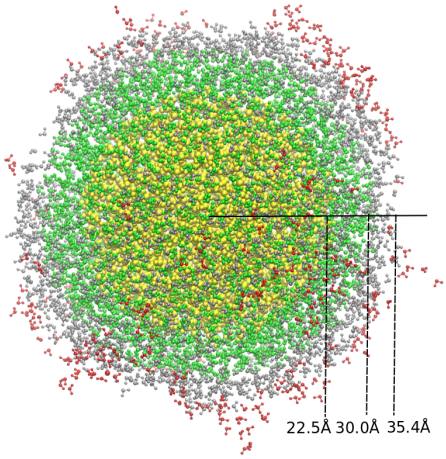

(b)

Figure 6: (a) Water density (blue line) and ion concentration (red line from simulations and black line from the solution of the non-linear Poisson-Boltzmann) of a droplet comprised 6130 water molecules and 20 Na^+ ions at $T = 300$ K. The blurry region delimits the error bars. The standard deviation is calculated by using 6 blocks of raw data, where every block has 2×10^4 configurations, separated by 0.2 ps. (b) Water spherical shells with center at the droplet COM. For clarity the Na^+ ions are not shown.

of the O sites at both temperatures. The H-DP crosses over the O-DP at $\approx$ 34.0 Å at both temperatures. The Na^+-CP shows a pronounced broad peak that has a maximum at 26.0 $\pm$ 0.5 Å. The region close to the maximum is found within the green colored region in Fig. 6 (b) (at both temperatures). As expected the Na^+-CP is broader at the higher temperature. We note the large error bars of Na^+-

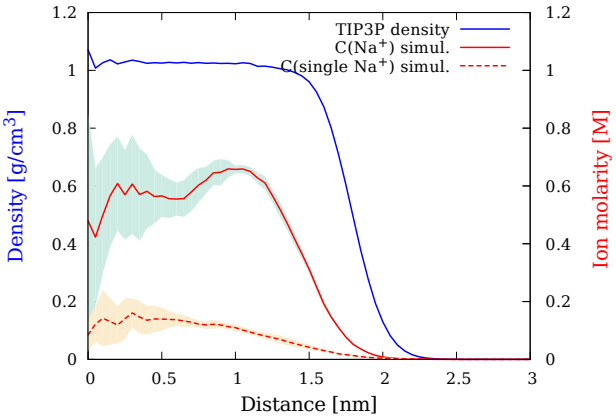

Figure 7: Water density (blue line) and ion concentration of a droplet comprised 880 water molecules, and 7 Na^+ ions (solid red line) and that of a droplet comprised 880 water molecules and a single Na^+ (dashed red line). The blurry regions delimit the error bars.

CP in 0 Å $< r <$ 17.0 Å (yellow colored region in Fig. 6 (b)). The poorer statistics arises from the fact that there are many more water molecules than ions, thus, the likelihood to encounter an ion at the center is very low. The integral of the raw histogram data (no division with the volume of the spherical shell) yields that 19.8 out 20 Na^+ ions at $T = 300$ K and 17.4 out of 19 Na^+ ions (one Na^+ evaporated) at $T = 350$ K are found at $r > 17.0$ Å. The histogram of the raw data of the distances of oxygen sites from the droplet COM show a maximum value at $r = 30.8$ Å, which is slightly shorter than that of the corresponding pristine droplet, which is at $r = 31.5$ Å. The maximum population of the oxygen sites (raw data) is at 28.3 Å$< r <$ 32.3 Å. The raw data of the Na^+ distances from the COM show a broad maximum at 26.0 Å$< r <$29.1 Å, thus they are within the region of the maximum oxygen population.

Figure 7 shows the Na^+-CP of droplets that comprise 880 water (TIP3P) molecules and (a) 7 Na^+ ions and (b) a single Na^+ ion. The simulations show that the concentration of a single Na^+ is higher in the interior ($r < 1.5$ nm) of the droplet and decays towards its surface. The location of the single Na^+ ion is consistent with previous studies in smaller clusters.[1,3,4,6,7] Electrostatic theory, based solely on the energetic

factor, predicts that a point charge will be located at the center of a dielectric medium with higher dielectric constant than the surrounding medium.[67] Simple ions are not point charges, thus, the predictions of electrostatic theory is not always sufficient to determine the ion location. Factors such as the ion size and ion-solvent charge transfer may play a role in determining their location in a droplet. The simulations show a broad single Na^+-CP in the droplet interior, which arises because of the thermal motion of the droplet constituents (entropic factor). Thus, the location of the single Na^+ follows the predictions of electrostatics on the fact that the ion is located in the droplet interior, but as expected, the Na^+-CP in the interior will be broad because of thermal motion.

The fact that the multiple charge carriers, Na^+ in our study, are not exactly on the droplet surface is consistent with the discussion in J. D. Jackson textbook[67] (3rd Edition, pp. 20): "At the microscopic level the charge is not exactly at the surface and the field does not change discontinuously." The formation of the Atkins "snowball"[68–70] around seed ions in liquid helium shows that even solvents with low polarizability polarize around the ions so as the ions are not exposed to the vacuo. The solvated hydronium[8–11] deserves a separate study. Based on our previous study[71] we think that the solvation energy over the charge density squared determines the solvation patterns of a spherical macroion. The charge itself increases the degree of hydrophilicity of an ion favoring solvation. The size of the ion will play an important role in determining their location. For instance, a highly hydrophobic macromolecule, such as a carbon buckyball, with charge $+e$ may lie mainly on the droplet surface (exposing a large part of their surface to vacuo) and travel occasionally a few solvent shells toward the interior[72–74] (this is to be contrasted with the single Na^+-CP discussed above). As expected the degree of hydrophobicity of the macromolecule in combination with its charge density plays significant role in determining its location.

It is in order to compare our findings with the ion-CP found in previous works. Our ion CP are substantially different from that presented in Fig. 3 of Ahadi et al. [16] for ≈ 1245 SPC/E water molecules. The droplets of 880-980 TIP3P H_2O molecules in this study are comparable in size to those in Ahadi et al. [16] study. Figure 3 shows[16] a spatial distribution of ions that is zero at $r < 4$ Å and it is very close to the water distribution at $r > 21$ Å. The ion and the water distributions diminish together. Moreover, the distributions of the ions, at the maximum in Ahadi et al.[16] is significantly more narrow than what we find. Similarly, the single ion distribution is different from our finding. In Ahadi et al.[16] the single ion does not approach the droplet COM. These differences may be attributed to the considerably different length of simulation times. In Ahadi et al.[16] the simulation time is 1 ns, while the simulations in this article are for 24 ns-60 ns. In the simulation set-up of Ahadi et al. the cluster was placed in a vacuo while in the present study it is placed within a large cavity, where the cluster is in equilibrium with its vapor. In vacuo, longer runs will lead to significant cluster evaporation and thus, an equilibrium ion distribution cannot be sampled. In Ahadi et al.[16] the lack of ion density in the center of the droplet is attributed in a qualitative manner to "entropic buoyancy". Since we found a non-negligible ion concentration in the droplet center, we cannot have a similar argument about the entropy effect. On the contrary, our study shows that entropy leads to a broadening of the ion spatial distribution relative to the predictions of electrostatics. As we are going to discuss in the following section the spatial distribution of the multiple Na^+ ions in a droplet can be explained by a combination of three factors, which are: the size of the ion, the droplet shape fluctuations and a Debye length.

Znamenskiy et al.[15] simulated a droplet comprised ≈ 4500 TIP3P H_2O molecules and 23 hydronium ions. It was found that the protons are distributed in three spherical layers around the centre of the droplet with fewer protons on the surface. Similarly to the study of Ahadi et al.[16] no proton distribution was found in a region (approximately 1 nm radius) from the centre of the droplet. The two layers closer to the center showed a significantly higher probability for the location of the hydronium ions than the outer

(nearest to the surface) layer. Even though we cannot directly compare the Na^+-CP with the hydronium distribution we think that the majority of the hydronium ions will be very near the surface and more toward the exterior than the Na^+ ions. We base our conjecture on the many studies of a single hydronium in small clusters[8–11] that show that the single hydronium ion is on the surface, and on the fact that in the droplets with multiple hydronium ions, the conducting nature of the medium favors the location of the ions on the surface. We expect to find hydronium density near the droplet COM, because as we discuss in the next section the general features of the ion spatial distribution can be captured by analytical theory.

Analysis of the ion spatial distribution in charged droplets

There are several factors that need to be considered when analyzing the ion distribution in a droplet.

In order to underline the causes affecting the ion distribution in a drop we start with a planar interface as an illustrative example. In an ideal conductor the potential inside the conductor is uniform and, using the Gauss' law, we find that the charge density in the interior is zero. Were the potential non-uniform the electric field will emerge. This will, in turn, induce constant flux of charge carriers. Nevertheless, the steady state is still possible. For such a steady state this flux has to be compensated by the counter flux due to the thermal diffusion of the charge carriers. In a droplet that contains ions of only one type, a relevant parameter describing the electrostatic interactions and the thermal diffusion is the Debye length (λ_D)

$$\lambda_D^2 = \frac{\epsilon k_B T}{4\pi n q^2} \tag{3}$$

where n is the ion number density (taken at the surface), $q = me$ (e is the elementary positive charge) is the charge of an ion, k_B is the Boltzmann constant, T temperature and ϵ is the dielectric constant. On small length scales, that are comparable with the Debye length, a good approximation to the charge distribution is obtained from the solution of the non-linear Poisson-Boltzmann (NPB) equation[75]

$$-\epsilon \Delta \Phi = qne^{-\beta[q\Phi]} \tag{4}$$

where on the interface $\Phi(0) = 0$. In Eq. 4, Δ denotes the Laplacian and Φ is the electrostatic potential. The solution of Eq.(4) is known[76] and has the following functional form

$$\tanh(\beta q\Phi(z)/4) = \tanh(\beta q\Phi(0)/4)e^{-z/\lambda_D} \tag{5}$$

where λ_D is the Debye length and z is the distance from the interface surface.

We are not aware of an explicit solution for the NPB equation in spherical geometry. For the spherical droplet we calculate the solution of the NPB equation using numerical methods by expanding the solution as a series of the Jacobi polynomials $P_k^{(-1,1)}$ of order $(-1, 1)$[17]

$$\Phi(r) = \sum \alpha_k P_k^{(-1,1)}(2r/R - 1). \tag{6}$$

and solving the equation iteratively. The solution of Eq. (5) yields the electric potential $\Phi(r)$ and the charge density distribution $q_{PB}(r)$.

The solutions for the electric potential in a sphere are remarkably well approximated by a single exponential. The ion distribution in the surface layer in the present model is highly non-uniform and the meaning of the ionic strength in this case should be altered to reflect this fact.

We calculated the electric potential profiles (Eq. 3) numerically using the GNU Scientific Library[77] for droplets comprising 10^3, 6×10^3 and 4×10^4 water molecules. We used the density value of 10^6[kg/m^3] to calculate the droplet radii reported in Table 1. The droplet charges were calculate using the Rayleigh limit ($X = 1$). We used the experimental value of $\varepsilon/\epsilon_0 = 80.0$ for the dielectric constant and $\gamma = 0.070$[N/m] for the surface tension. Equation (4) tacitly assumes that there are no counter-ions present in the droplet. Hence, for large droplets, calculations yield large values for the Debye length. However, this assumption is incorrect for intermediate droplet sizes and the resulting potential will show faster decay at the surface layer.

The electric potential and the ion concentration are connected by the Gibbs-Boltzmann distribution (see Fig. 9). For the droplet sizes used in the numerical modeling we observe that the ion concentrations between the droplet surface and the surface interior differ by less than an order of magnitude. In large droplets counter-ions will play an increasingly important role. The charge density in larger droplets at the Rayleigh limit will decrease and the corresponding Debye length will be larger. For certain sizes of droplets the Debye length will be determined by the ionic strength of the solution rather than the ion concentration on the surface.

Table 1: Results of numerical solutions of the NPB equation for critical charged droplets comprising $N_{\mathrm{H_2O}} = 10^3$, 6×10^3 and 4×10^4 water molecules. We provide a fitted value of the decay length λ_{fit} (third column) of the electric potential (5) at the surface. $\Delta\Phi$ (fourth column) is the potential difference between the center of the drop and its surface. Molar concentration, denoted by C, of the ions at the surface is reported in the last column.

$N_{\mathrm{H_2O}}$	r[nm]	λ_{fit} [nm]	$\Delta\Phi$ [V]	C [mM]
1000	1.93	0.68	0.035	200
6000	3.50	1.16	0.042	68
40000	6.59	2.03	0.051	23

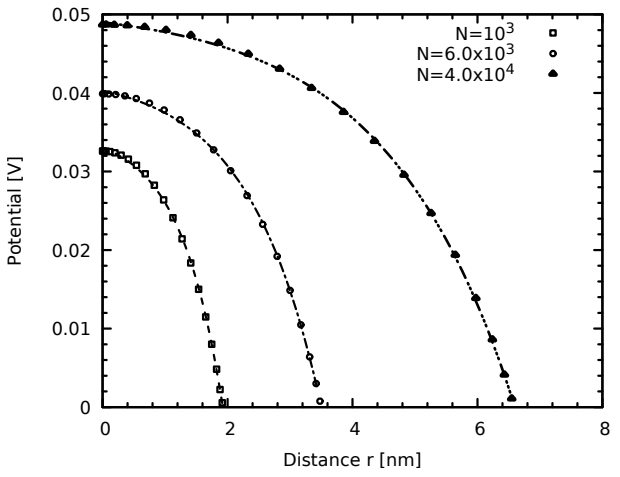

Figure 8: Profiles of the electric potential for droplets described in Table 1. We set the droplet potential at the surface to zero.

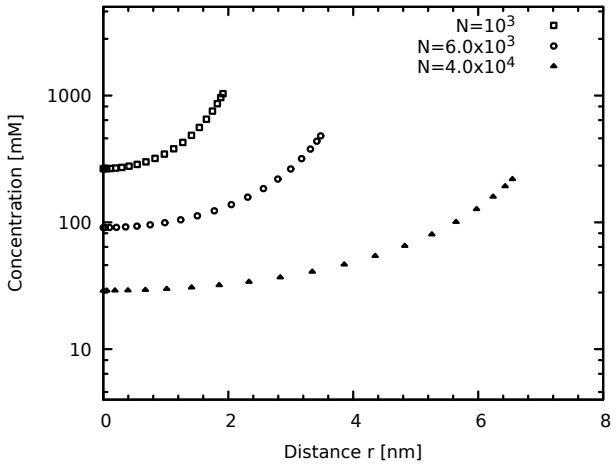

Figure 9: Molar concentrations of ions in the critical Rayleigh droplets as a function of the distance from the center for different droplet sizes. The droplet parameters are described in the text.

The solution of the NPB equation yields the distribution of the ions as a function of the distance (r) from the surface. This quantity differs from the distribution measured from the center of the droplet. In this case the charge distribution is attenuated by fluctuations of the interface. First, let us consider density fluctuations of the planar interface due to surface fluctuations. Given the interface $z(x, y)$ the average solvent density $\rho(z)$ is given by

$$\langle\rho(\zeta)\rangle = P(\zeta > z(x, y)) = \langle\zeta - \theta(z(x, y))\rangle \quad (7)$$

where θ is the Heaviside step function and the density is normalized as $\rho(-\infty) = 1$

On the other hand the charge distribution of a fluctuating surface can be approximated as

$$q(\zeta) = \langle q_{PB}(\zeta - z(x, y))\rangle = \langle \int d\tau\delta(\zeta - z(x, y) - \tau)q_{PB}(\tau)\rangle \quad (8)$$

In the r.h.s. of the equation we introduced the Dirac delta function in order to integrate the last integrand by parts and replace the Dirac function with the Heaviside θ function and reduce the integral to the convolution of the number density and the derivative of the Poisson-Boltzmann charge distribution. After some algebra we arrive at the following expression for

the charge density of the fluctuating surface:

$$q(\zeta) = \langle q_{PB}(\zeta - z(x,y))\rangle = q_{PB}(0)\rho(\zeta) - \int d\tau \rho(\zeta-\tau) q'_{PB}(\tau) \quad (9)$$

We emphasize that Eq. (9) is exact only for fluctuating planar interfaces. In the interior of droplets we expect Eq. (9) to be only qualitatively correct.

The last factor to consider is the size of solvated ions. It is energetically highly unfavorable for an ion to be located at the surface of a drop. The simulations demonstrate that an ion does not approach the surface of a droplet closer than this length. In Fig. 6 we show the ion distributions obtained from Eqs. (5,9) (black solid line) and the CP from simulations (red solid line). We used 3 Å radius for the size of the sodium ions. As expected, the simulated and theoretical profiles agree in the vicinity of droplet surface and show some deviations in the droplet interior. The results presented in Fig. 6 demonstrate that the finite size of a solvated ion, fluctuating interfaces and the Debye theory describe all the features of the ion distribution in the charged droplets.

Water dipole orientation

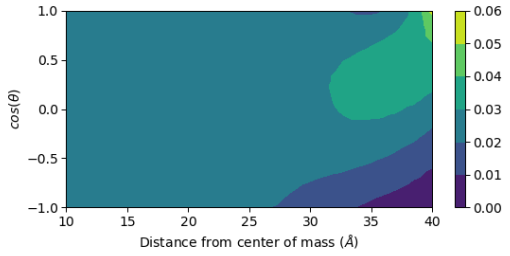

Figure 10: Same as Fig. 3 but the droplets comprised 6139 TIP3P H_2O molecules and 20Na^+ ions. The droplets are at $X = 0.9$ (Eq. 2).

Similarly to Fig. 3, Fig. 10 shows the $\cos(\theta)$ distribution as a function of the distance from the droplet COM (r). The $\langle \cos\theta \rangle$ is shown in Fig. 4. Here, we discuss the $\cos(\theta)$ distribution of a droplet comprised 6139 TIP3P H_2O molecules and 20 Na^+ ions at $T = 300$ K. The $\cos(\theta)$ distributions within representative spherical shells (with center at the droplet COM) for a droplet comprised $\approx$ 1000 and an $\approx$ 6000-H_2O-molecule droplet with Na^+ ions at $T = 300$ K and 350 K are shown in Figs. S9 and S10 in the supplementary material. The general features of the distributions are: (a) in the charged systems the $\cos(\theta)$ distribution is shifted toward positive values as shown in Fig. 4; (b) the dipole orientation due to the ions is propagated both in the interior and outer layers. In the inner layers a preference in the dipole orientation reaches the droplet center (it is only within a sphere of $r \approx 2.5$ Å that the $\cos(\theta)$ distribution appears to be uniform but with large fluctuations relative to the pristine droplet) (c) the water dipoles are strongly oriented within 17.0 Å $< r <$ 28.5 Å which is the shell with the highest density of Na^+ ions; (d) In the outer shells up to $r \approx 40$ Å the $\cos(\theta)$ distribution is broad in the positive values and $\cos(\theta) = 1.0$ is not the maximum; (e) At $r \geq 40.0$ Å, where the density of water is minimal the dipoles are strongly oriented with $\cos(\theta) = 1.0$ because of the overall droplet charge and not that of the individual Na^+ ions. Figure 4 shows that the $\langle \cos\theta \rangle$ in the sodiated droplets follows the same trend as in the pristine ones but in the sodiated droplets the $\langle \cos\theta \rangle$ is shifted more toward the positive values.

In more detail the $\cos(\theta)$ distribution is as follows: In a spherical shell of r =2.5 Å the $\cos(\theta)$ distribution averages to zero and is uniform for both droplet sizes. At r >2.5 Å there is a gradual shift toward the positive $\cos(\theta)$ values. At $r = 10 \pm 0.5$ Å there is a modest shift toward positive $\cos(\theta)$ values especially in the range of $0.45 - 1$. At $r = 15 \pm 0.5$ Å there is a moderate shift toward positive $\cos(\theta)$ values in the range of $0.80 - 1$ (20% higher population with $\cos(\theta)$ +1 than −1). Now, we shall examine the features of the angle distribution at 17.0 Å $< r <$ 28.5 Å, which is the interval where the probability density of Na^+ ions is the highest. At $r = 17.0 \pm 0.5$ Å even though all the angles are substantially populated, the higher $\cos(\theta)$ values are increasingly populated and the maximum is at $\cos(\theta) = +1$. The population of H_2O molecules with $\cos(\theta) = +1$ are $\approx$ 20%

more than those with $\cos(\theta) = -1$. At 25.0 Å $< r <$ 26.0 Å the increase of the population of the positive $\cos(\theta)$ values in the range $0.75-1.0$ (40% higher $\cos(\theta) = +1$ population than -1) becomes more pronounced. At $r = 28.5 \pm 0.5$ Å the $\cos(\theta)$ distribution is strongly shifted toward the positive values where a broad range of angles with $\cos(\theta)$ values $0.5 - 1.0$ (which corresponds to angle range $60° - 0°$) are highly populated. The $\cos(\theta) = 1$ has a marginal maximum population. For 29.0 Å $< r <$ 39.0 Å $\cos(\theta) = 1$ is highly populated but it is not the maximum as in the smaller r. The maximum $\cos(\theta)$ value shifts gradually toward the range of $0.25 - 1.0$ at $r = 29 \pm 0.5$ Å, to $0.0 - 1.0$ (almost uniform distribution) at $r = 30 \pm 0.5$ Å, to $0.0 - 0.50$ at 32 Å$< r <$ 34 Å. Close to $r = 34$ Å the angles are in the range of $66° - 90°$ with the maximum found at 75° ($\cos(\theta)$) = 0.25). At 37.0 Å $< r <$ 38.0 Å the highest $\cos(\theta)$ population is in the range $0.25 - 1.0$, which shows an almost uniform distribution. For $r \approx 39.0$ Å there is a strong preference for larger $\cos(\theta)$) values in the range of $0.50 - 1.0$. The population is approximately 50% more for the droplet at $T = 350$ K than at $T = 300$ K. We attribute this difference to the fact that the lower temperature droplet is less extended than the higher temperature as shown in Fig. S6 in the supplementary material. For $r \geq 40.0$ Å, where the dipole population is minimal, there is a clear preference for $\cos(\theta) = 1.0$. These water molecules are far away so as they view the rest of the droplet as a central charge. At this distance the conducting or dielectric character o f the droplet does not play a role.[18] Several comments regarding the orientation of the outer water molecules are in order. We remind that in the outer layers there is a rapid decrease in the water density. At $r >$ 39 Å there are on the average 44 H_2O molecules and at $r >$ 40 Å there are 22 H_2O molecules. As shown in Fig. 4 these few molecules are strongly oriented. Conceivably, these H_2O molecules cannot cover the entire surface but they form islands on the more compact surface. These islands have the form of dangling oriented strings that can be as long as 4-5 H_2O molecules. The strings disintegrate and reform and they undergo elastic motions, which are reminiscent to those of the "rays" of the "star"-shaped droplets.[18,21] We also need to consider that the perfect dipole orientation in the outer and inner layers (grey shell in Fig. 6) is prevented by the molecule thermal motion. In the outer shells the thermal motion causes an elastic collective motion[18,21] in the dangling surface chains. In summary, simulations show that in the outer droplet layers, but also in the droplet interior there is an overall shift towards $\cos(\theta) > 0$. However, there is not a close alignment between $\vec{r}$ and the water dipole because of several factors: (a) the thermal motion of the dipoles competes with a perfect alignment; (b) the water molecules are not symmetrically surrounding a Na^+ ion; (see Fig. S8 in the supplementary material) and (c) the orientation of the water molecules are affected by the significant variations in density within a droplet, the existence of the free surface, and the presence of multiple ions that may affect the orientation of the intervening water molecules between them. All these factors will play a role in the manner in which the water molecules are oriented. Because of these factors we consider that the picture of a cascade of orientations initiated from the ions and induced in sequence to the solvent molecules up to the surface[16] is inaccurate. As we discussed, the outer water molecules are oriented by the entire droplet charge and not by the specific ions. We cannot also ignore the fact that throughout the shells there is a significant number of molecules with negative $\cos(\theta)$ values, thus, the average $\cos(\theta)$ tends toward unity only at the very dilute shells as shown in Fig. 4. A question that has been posed in the literature by many scientists (see for instance[16]): "does the charge of the ions transfer to the surface"? Based on the above discussion, we think that the surface of a droplet has a percentage of oriented dipoles (both in the interior and the outer shells) because the droplet is overall charged. The very outer molecules (dangling short chains of water), which are very few will be strongly polarized because of the entire charged droplet. If we consider these very few surface molecules (for instance a few tens for a 6000-H_2O molecule droplet) and also a degree of dipole orientation in the more compact

surface, it appears that that there is no reason for the charge right on the surface to be equal to the total charge of the ions. As we discuss in the next section, a droplet of the same size and of the same amount of charge, but with the charge distributed on a polyhistidine and Na^+ ions, yields identical orientation of the water dipoles to that of Na^+ ions. This similarity indicates that it is the overall droplet charge that determines the orientation of the dipoles. In addition, the three aformationed factors will play a role on determining the charge on the surface. Ahadi et al.[16] concludes that all the charge of the ions transfers on the surface because of the orientation of the dipoles as evidenced by electrostatic maps that the authors have computed. The electrostatic maps are not provided in Ahadi et al. article,[16] hence, we cannot compare with our findings.

Electric field on the molecular surface

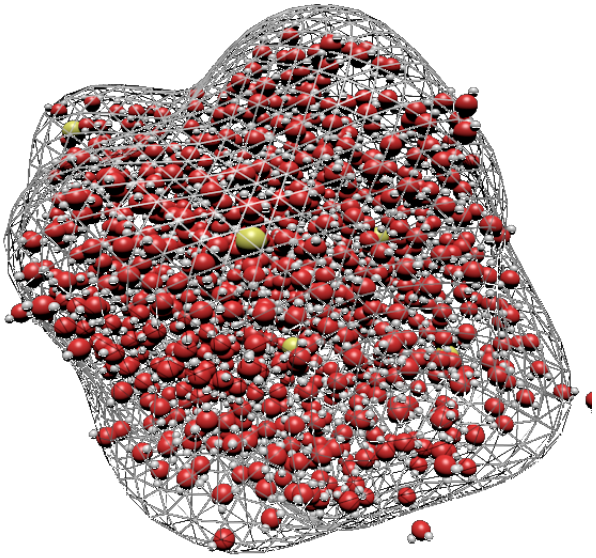

Figure 11: Reconstruction of the droplet surface using the spherical harmonics amplitudes from Eq. (14). The low order perturbations are well reproduced unlike string-like transient structures on the surface.

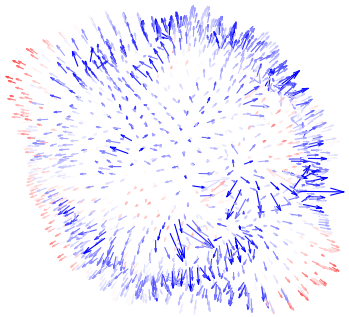

Figure 12: Interpolated electric field of the molecular surface of the droplet. The arrows represent the direction and the magnitude of the electric field on the surface. The arrows are color coded according to the value of the electric potential from red (1V) of the extruded domains of the droplet to blue (1.5V) on the areas of the surface that are closer to the droplet center.

The Rayleigh derivation of the stability limit ($X = 1$ in Eq. 2) for a conducting droplet relies on the properties of a conductive medium.[41–44] These properties are that the electrostatic potential on the surface is a constant and that the charge is localized at the surface. Using the Gauss law[67] we can identify the surface charge density using the normal component of the electrostatic field (E_n). The tangential component E_t is equal to zero. The normal component of the electric field enters the Born model of the ion evaporation.[78,79]

We attempted to test the equipotentiality condition on the molecular surfaces of the droplets that we simulated. There are a number of obstacles in computing the electric field on the surface of a droplet. Fast dynamics of the solvent molecules on the surface changes the droplet shape. Thus, the partial charges on the ions and on the solvent molecules lead to highly varying values of the electric field of up to a

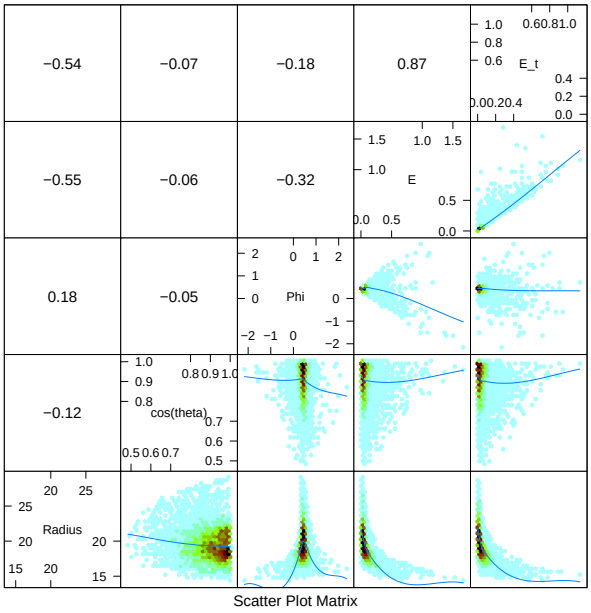

Figure 13: Statistical analysis of the factors correlating with the value of the electric potential on the surface. In the plot a correlation matrix among data columns sampled on the surface of the droplet is shown. The columns comprise radius from the center of mass (Radius [Å]), cosine of the angle between the radius vector and the normal to the surface at this point (theta), value of the electrostatic potential (Phi [V]), magnitude of the electric field(E [V/Å]) and magnitude of the tangential component of the electric field (E_t [V/Å]). The diagonal shows the histograms of the values from the different columns. In the upper triangular matrix the values of the Pearson correlation matrix are shown. The lower triangular matrix contains scatter plots of the pairs of columns.

nanometer distance from the surface precluding the calculation of the equipotential electric surface. Therefore, one can not use averaging to obtain meaningful statistics of the value of electric potential on the surface. For this reason we follow a different approach.

We assume that the surface can be expressed as

$$r(\vartheta,\phi) = R + \sum_{l>0,m} a_{l,m_l} Y_{l,m}(\vartheta,\phi) \qquad (10)$$

where, (ϑ,ϕ) is the spherical angle, $r(\vartheta,\phi)$ is the distance from the droplet centre, $Y_{l,m}(\vartheta,\phi)$

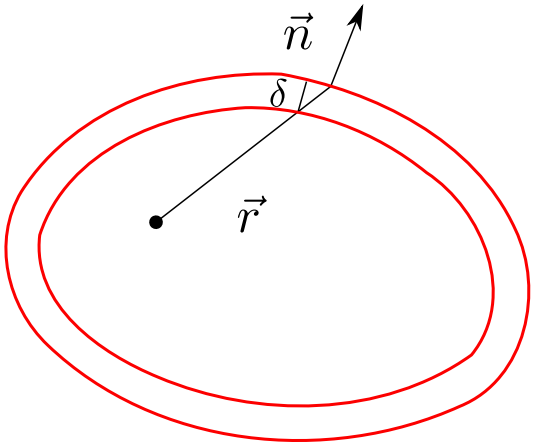

Figure 14: Illustration of the change in the radius vector when the surface is offset by a fixed distance δ.

are the spherical harmonic functions of rank m and order l, $|m| \leq l$ and $a_{l,m}$ are the expansion coefficients (we call them amplitudes). R is the $l = 0$ term in the expansion of $r(\vartheta,\phi)$. This expansion can be used, for instance, in the case of convex shapes. Hereafter, we use the following notation

$$\delta r = \sum_{l>0,m} a_{l,m} Y_{l,m}(\vartheta,\phi). \qquad (11)$$

We compute the values of the amplitudes of the expansion of the droplet surface first, by calculating the expectation value of the complex conjugate of a spherical harmonic $(Y^*_{l,m})$ for every pair (l,m), where $l > 0$ and $|m| \leq l$.

$$\langle Y^*_{l,m}(\vartheta,\phi)\rangle = \frac{1}{M}\sum_i m_i Y_{l,m}(\vartheta_i,\phi_i). \qquad (12)$$

where the asterisk signifies the complex conjugate function, m_i is the mass of every atomic site and M is the total mass of the droplet.

If we assume that the mass density of the droplet is uniform we can express the expectation value of the spherical harmonics using the

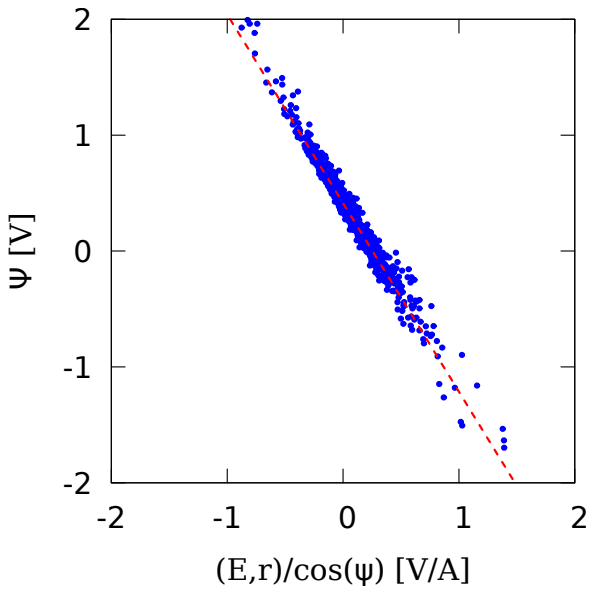

Figure 15: Scatter-plot of the values of the potential on the surface and its derivative in the direction of the radius vector $(\mathbf{E}, \hat{\mathbf{r}})/\cos\psi$.

integration over volume

$$\langle Y^*_{l,m}(\vartheta,\phi)\rangle = \frac{\rho}{M}\iiint\limits_{t\le r(\vartheta,\phi)} Y^*_{l,m}(\vartheta,\phi)t^2dt\cos(\vartheta)d\vartheta\phi = \frac{1}{4\pi R_0^3}\iint r(\vartheta,\phi)^3 Y^*_{l,m}(\vartheta,\phi)\cos(\vartheta)d\vartheta\phi \quad (13)$$

where ρ is the average droplet density and R_0 is the radius of a spherical droplet. To do the integration in Eq. (13) we use Eq. (10) for the value of the radius $(r(\vartheta,\phi))$ and expand its third power as a series. From the orthogonality property of the spherical harmonics we obtain the average of the spherical harmonics

$$\langle Y^*_{l,m}(\vartheta,\phi)\rangle = \frac{3R^2}{4\pi R_0^3}\alpha_{l,m}. \quad (14)$$

In the remainder of the section we assume that the droplet radius is given by the radius of the unperturbed droplet, i.e. $R \approx R_0$.

We calculate the droplet radius from the value of the radius of gyration (R_{Gyr})

$$R_0^2 = \frac{5}{3}R^2_{\mathrm{Gyr}}. \quad (15)$$

Combining equations (14) and (15) we arrive at the following *key equation* for the molecular surface:

$$r(\vartheta,\phi) = \sqrt{\frac{5}{3}}R_{\mathrm{gyr}}\left[1+\frac{4\pi}{3}\sum_{l>0,m}\langle Y^*_{l,m}(\vartheta,\phi)\rangle Y_{l,m}(\vartheta,\phi)\right] \quad (16)$$

For a charged droplet we express the value of the electric potential $(\Phi(r,\vartheta,\phi))$ using the multipole expansion

$$\Phi(r,\vartheta,\phi) = \frac{Q}{4\pi\epsilon_0 r} + \sum_{l>0,m}\frac{t_{l,m}}{r^{l+1}}Y_{l,m}(\vartheta,\phi) \quad (17)$$

where Q denotes charge and $t_{l,m}$ are the expansion coefficients. We calculate the $t_{l,m}$ by using the orthonormality conditions of the spherical harmonics. We evaluate the value of the electric potential (Φ) on the mesh given by Lebedev quadrature (see e.g.[80]) and compute the weighted sum

$$\frac{t_{l,m}}{R^{l+1}} = \sum_k w_k \bar{Y}_{l,m_l}(\vartheta_k,\phi_k)\Phi(R,\vartheta_k,\phi_k). \quad (18)$$

Eq. (18) is exact up to order l given by the order of approximation of the Lebedev quadrature. The expansion (17) is unique, however, it has to be truncated or regularized. Calculation of the electric potential using the expansion (17) diverges near the molecular surface due the presence of the solvent or ionic charges. In the numerical experiments we have truncated the expansion at order 8.

We calculated the values of the electric potential and of the electric field for an aqueous droplet comprising eight Na^+ ions and $\approx$ 980 H_2O molecules. The total length of the trajectory was 60 ns and during the simulations the drop stayed intact with few water molecules evaporating. A representative connected cluster with the reconstructed molecular surface is shown in Fig. 11. The electric field is computed as the numerical derivative of the electric potential. A sample of the electric field on the surface of the droplet is shown in Fig. 12. We observed that the molecular surface calculated

for a charged droplet deviates from the iso-potential surface interpolated using Eq. (17). In Fig. 13 we show the results of the statistical regression testing of a number of variables recorded on the surface of the droplet.The analysis has been performed using the *R Statistical Analysis Package* version 3.4.1.[81] The results of the regression analysis shows that none of the factors such as value of the electric field, angle of the normal to the surface, surface distance to the center can account for the deviation from the iso-potentiality condition.

We believe that the main cause for this is the size of a solvated ion. If the size of a solvated ion is δ then the molecular surface has to be offset by $\delta/(\hat{\mathbf{n}}, \hat{\mathbf{n}})$, where $(\hat{\mathbf{n}}, \hat{\mathbf{n}})$ is the cosine of the angle ψ between the normal to the surface and the radius vector. We can approximate the value of the electric potential using the following equation

$$\Phi(\mathbf{r}) - \Phi(\mathbf{r}') = -(\mathbf{E}, \mathbf{r} - \mathbf{r}') = -\frac{\delta}{\cos\psi}(\mathbf{E}, \hat{\mathbf{r}}) \tag{19}$$

In Fig. 15 we plot values of the electric potential against its directional derivative $(\mathbf{E}, \hat{\mathbf{r}})/\cos\psi$. We observe strong correlation between the data. Using linear regression we determined the maximum likelihood value of the offset $\delta = 1.7$Å of the molecular surface potential that would have equal values of the interpolated electric potential. The offset is smaller than the typical distance of a sodium ion from the surface (see Fig. 7 for the distance from the surface) indicating that it is the solvated ions are the active charge carriers in the aqueous droplets.

It is rather unexpected that an instantaneous molecular surface satisfies iso-potentiality condition for an interpolated potential with an offset. We would surmise that this fact is a major reason why the Rayleigh criterion holds for small charged droplets.

Polyhistidine in a conducting droplet

Typical snapshots of droplets comprised ≈ 6000 H_2O molecules, ≈ 10 Na^+ ions and a polyhistidine His_{10}^{10+} and His_{20}^{10+} are shown in Fig. 16 (a) and (b), respectively.

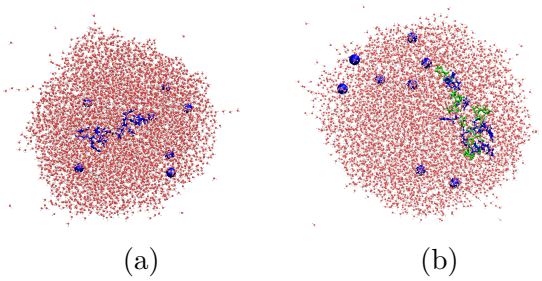

(a) (b)

Figure 16: Typical snapshots of an aqueous droplet comprised ≈ 6000 H_2O molecules and 10 Na^+ ions (blue spheres) and (a) His_{10}^{10+} (blue chain) and (b) His_{20}^{10+} (blue and green colored chain). For the rest of the molecules the color coding is the same as in Fig. 1.

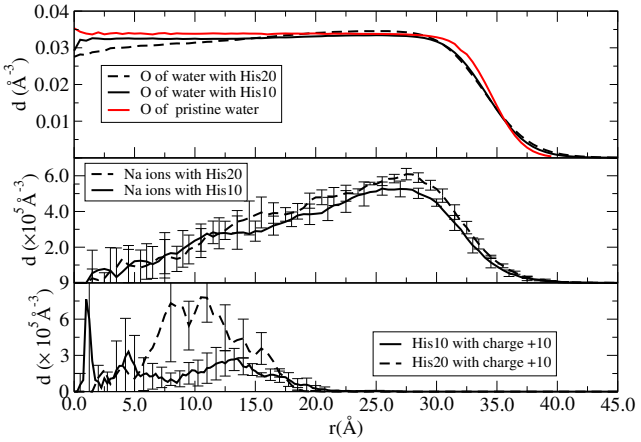

Figure 17: Upper panel: Density (d) of oxygen sites of H_2O molecules as a function of r in pristine droplets and droplets with the polyhistidine comprised ≈ 6000 H_2O molecules. Middle panel: d of the Na^+ ions. Lower panel: d of His_{10}^{10+} and His_{20}^{10+}. For the histograms of His_{10}^{10+} and His_{20}^{10+}, 5×10^4 configurations collected every 0.2 ps and a bin size is 0.5 Å were used. The density is in units of of $\mathring{A}^{-3} = 1.66 \times 10^6$mM.

Figure 17 shows the DP of oxygen sites of H_2O molecules (upper panel), that of Na^+ ions (middle panel) and that of His_{10}^{10+} and His_{20}^{10+} (lower panel).

For $r > 29.0$ Å, the decrease of the oxygen (and hydrogen) profiles is smooth as expected

because of (a) the droplet shape fluctuations and (b) the reduction of the H_2O density on the droplet surface that lead to a rough surface with dangling short chains of H_2O molecules. The distribution of the Na^+ ions shows a broad peak at 25.0 Å$< r <$28.0 Å, which is approximately 4 layers of water under the vapor-liquid interface (the diameter of a TIP3P H_2O molecule is 3.15 Å). The outer water layer is not a complete shell and moreover, it is characterized by roughness, lower density and fast diffusion. As it is shown, the Na^+ distribution also decreases smoothly (at distances $\approx$ 28.0 Å), which indicates that the Na^+ ions can also be found with small probability very close to the surface. Very close to the center of the droplet, we can find a very low density of Na^+ ions.

His_{10}^{10+} is more likely to be found close to the center of the droplet and it diffuses up to $\approx$ 25.0 Å from the droplet COM. Interestingly, His_{10}^{10+} may diffuse up to the distance where the Na^+ profile has its maximum. We note here that the His_{10}^{10+}-DP is built with respect to its COM, thus the end of the chain may be found closer to the surface than the distance of the polyhistidine center of mass. His_{10}^{10+} has a very high degree of hydrophilicity primarily because of its high charge and secondarily because of the polar sites of polyhistidine. The fact that His_{10}^{10+} travels very close to the surface even though very hydrophilic is not surprising. The location of the His_{10}^{10+} is consistent with the conducting properties of the droplet.

When His_{10}^{10+} resides close to the surface the droplet obtains a slightly prolate shape and the Na^+ ions move on the opposite site of the droplet. Because of this movement the droplet fluctuates between a prolate and spherical shape as we observed several times. It is still to be examined whether such fluctuations occur also in much larger droplets, and whether they may divide the droplet. The location of His_{10}^{10+} in the aqueous droplet in the presence of Na^+ ions is to be contrasted to its location in a dielectric aqueous droplet where the charged polyhistidine resides in the center of the droplet as we have found in our previous work.[18]

The His_{20}^{10+}-DP shows that it may be found close to the droplet COM. Evidence of the His_{20}^{10+} location is also shown in the oxygen-DP in the upper panel of Fig. 17, where there is depletion of the water molecules close to the droplet COM. His_{20}^{10+} may diffuse close to the region that the density of the Na^+ ions is maximal. The His_{20}^{10+}-DP shows that the His_{20}^{10+} may be found closer to the surface than the His_{10}^{10+} since His_{20}^{10+} is characterized by lower charge density than His_{10}^{10+}.

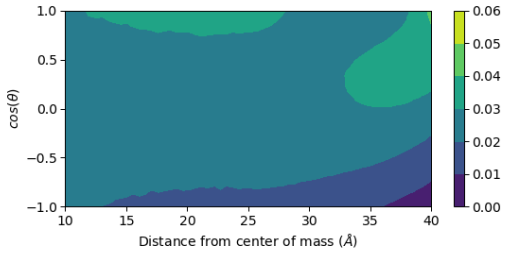

Figure 18: Same as Fig.3 but for a droplet composed of 6000 H_2O molecules, His_{10}^{10+}, and 10 Na^+ ions (3 have evaporated) at $T = 350$K. For the histograms, 50000 configurations collected every 0.2 ps and a bin size is 0.5 Å were used.

Figure 18 shows the probability of $\cos(\theta)$ as a function of r. Clearly we see a positive shift in the $\cos(\theta)$ distribution, which is similar to that of a droplet with 20 Na^+ ions (see Fig. 10 and Fig. S10 in the supplementary material). It is surprising that the considerably different charge distribution does not affect the orientation of the dipoles. This similarity indicates that it is the overall charge in the droplet and other factors mentioned in the previous section that determine the dipole orientation.

In the following discussion we relate our findings to the processes that may occur in droplets generated in ESI experiments. Recurrent questions in ESI-MS is how a macroion acquires its charge state and how it emerges from the droplet. Even though, we do not use a dissociative molecular model that will allow us to see the charge transfer, the analysis provides certain insight. Firstly, we find out that a highly charged hydrophilic macroion can reside for a short period of time close to the surface. The reason for its surface locality is the fact that the droplet with free ions is a conductor, thus, the charge will be mainly on the surface. Secondly,

even though we have not studied the effect of solvent evaporation in this article, we think that evaporation of a droplet assists in bringing a macroion closer to the surface because layers of water are removed. We remind here that in an initial electrosprayed mist of droplets, a macroion can be found anywhere in the droplet because the initial droplet state is not at equilibrium. It is more likely that the macroions and the ions (in this non-equilibrium state) are found in the outer layers of the droplet, because of the more available area. In order to analyze the locality of the macorion, the solvent evaporation rate is to be compared with the macroion's diffusion rate. A typical protein diffuses approximately by one nanometer per nanosecond. The diffusion in droplets, which are mesoscopic clusters may be also assisted by shape fluctuations, thus the diffusion rate may be different from that reported for bulk solution. The evaporation rate of a droplet depends on several factors[82,83] and it slows down as the droplet radius decreases. Our previous computations have shown evaporation rate of approximately 52 H_2O molecules per nanosecond for a droplet[50,84–86] of a radius of ≈ 3.6 nm at T =300 K.[85] Within one nanosecond, the droplet radius may decrease by two shells of water. Thus, at a temperature close to the room temperature the diffusion of the macroion will distance it from the surface faster than approaching the surface due to the the reduction of the droplet size. In principle, we should be examining the effect of evaporation in the location of the macromolecule at a much larger droplet than that that can be simulated at the atomistic level. We still need to examine the outcomes of a high non-equilibrium scenario where the solvent evaporation rate is high. It is possible that under high evaporation rate a macroion with high degree of hydrophilicity will be found close to the surface and extrude.[50,71]

In summary, a macromolecule even with a high degree of hydrophilicity may be found occasionally near the surface of the droplet. The macroion locality may affect its charge state, since the shells near the surface have a higher ion concentration. The evaporation rate is expected to play a significant role in the mechanism of macroion release. If the solvent evaporation rate is higher than the macroion diffusion rate, then, charge (commonly protons) may transfer on the surface of the macroion and then, the macroion can possibly extrude from a droplet. The role of a high evaporation rate on the release mechanism of highly charged macroions deserves its own study.

Conclusion

We examined the spatial distribution of simple ions and that of a mixture of simple ions and macroions in highly charged aqueous droplets. We found that in aqueous droplets comprised simple ions at an overall charge state slightly below the Rayleigh limit ($X \approx 0.8 - 0.9$) the concentration of the ions is higher close to the surface. Non-negligible concentration of ions was found up to the droplet COM. In the interior there is only one ion but the density is significant because the volume is smaller than that of the outer solvation shells. We think that ions are found in the interior because regardless of the value of the electric field in the interior (ideally the electric field is zero for a conductor) the ions diffuse because of Brownian motion. We have proposed an analytical theory that captures all the general features of the ion spatial distribution.

Our findings and interpretation of the ion distributions are different from previous studies[15,16] as explained in the analysis of the data. In the presence of charged peptides with high degree of hydrophilicity we find that the peptide density is higher in the interior, but it still diffuses near the surface, where the majority of the single ions are found. We think that the reason that the charged peptide is found in the interior relative to the single ions, is its high charge density. In the nanodrops that we studied, we saw the droplet prolate-spherical fluctuations as the macroion diffuses closer to the surface. The diffusion may be assisted by the droplet shape fluctuations due to its high charge. It is still to be examined whether such fluctuations appear in larger droplets and whether they may possibly rapture the droplet. Yet, we think that the

larger the droplet, the less pronounced the fluctuations are relative to the size of the droplet.

We found that in droplets of the same size and charge, different charge distributions polarize the water dipoles identically. In this study we compared the case where charge $+20\ e$ is carried by 20 Na^+ ions with that that the charge is distributed between a macroion ($+10\ e$) and simple ions ($+10\ e$). This finding indicates that the amount of charge transferred to the droplet surface by the orientation of the water dipoles is determined by the overall charge of the droplet and also by other factors such as the thermal motion of the dipoles that competes with the dipole alignment, the existence of the free surface and the significant density variations within the droplet.

We computed the electric potential and electric field close to the droplet surface. We found that an equipotential surface is found in the interior of a droplet at a distance 1.7 Å from its surface. The findings indicate that the active charge carriers are the Na^+ ions surrounded by the immediate water shells. We suggest that we may have to consider a smaller radius in the Rayleigh expression for a droplet. The correction may not be very large but it may give insight into the molecular interpretation of the Rayleigh limit. This interesting theoretical finding deserves further investigation in future articles.

We propose that for non-equilibrium simulations of droplets which are related to ESI-MS, it is more natural to initiate the production runs by placing the macroion in an intermediate water shell or closer to the surface rather than in the droplet center as it is routinely done. In this way one may examine the simulation outcomes determined by the competition between solvent evaporation rate and macroion diffusion rate.

Some of the findings related to the orientation of the surface water may be force field dependent as already has been discussed in the literature.[54] In this article we emphasize general features of the ion distribution in droplets supported by theory and by comparison of different charge distributions and thus, they do not depend on the details of the force field. It is interesting to also examine by simulations and analytical theory the distribution of the negative ions, multi-valent ions and the ion distribution in the presence of counterions. The surface tension of the charged droplets is another problem to be investigated. We have completed these studies and we expect to provide our findings in forthcoming articles. The applied modeling does not include the electronic polarization of the constituents and of course, it is desirable to look into the effect of polarizable force fields in the structure of the droplets.[5,87,88]

Supporting Information

See supporting information for additional analysis of (a) raw data of the population of oxygen sites in aqueous neutral droplets; (b) $\cos(\theta)$ distributions of water molecules in pristine and sodiated aqueous droplets; (c) typical snapshots of sodiated droplets comprised 1000 water molecules.

Acknowledgement S.C. thanks Prof. D. Frenkel, Department of Chemistry, University of Cambridge, Prof. R. Kapral, Department of Chemistry, University of Toronto and Prof. S. S. Xantheas, Pacific Northwest National Laboratory, for discussions and encouragement for continuation of this research. S.C. acknowledges discussions with Prof. P. Scheier, Institute of Ion Physics and Applied Physics, University of Innsbruck on the Atkins "snowball" and discussions with Prof. J. H. Futrell, Pacific Northwest National Laboratory, Prof. D. Clemmer, Department of Chemistry, Indiana University Bloomington, Prof. D. Russell, Department of Chemistry, Texas A& M University and Prof. E. Williams, Department of Chemistry, University of California at Berkeley on the fascinating world of mass spectrometry. Discussions with Ms. Zijie Xie, graduate student in the research group of Prof. E. Williams are acknowledged. V.K. and S.C. also acknowledge discussions with Dr. Myong In Oh and Dr. Mahmoud Sharawy (University of Western Ontario). S.C. acknowledges an NSERC-Discovery grant (Canada) for funding this research. Sci-Net, SHARCNET and Compute Canada are acknowledged for providing the

computing facilities.

References

(1) Stuart, S. J.; Berne, B. Surface curvature effects in the aqueous ionic solvation of the chloride ion. *J. Phys. Chem. A* **1999**, *103*, 10300–10307.

(2) Bush, M. F.; Saykally, R. J.; Williams, E. R. Infrared action spectra of Ca2+ (H2O) 11- 69 exhibit spectral signatures for condensed-phase structures with increasing cluster size. *J. Am. Chem. Soc.* **2008**, *130*, 15482–15489.

(3) Hagberg, D.; Brdarski, S.; Karlström, G. On the solvation of ions in small water droplets. *J. Phys. Chem. B* **2005**, *109*, 4111–4117.

(4) Perera, L.; Berkowitz, M. L. Many-body effects in molecular dynamics simulations of Na+ (H2O) n and Cl-(H2O) n clusters. *J. Chem. Phys.* **1991**, *95*, 1954–1963.

(5) Thaunay, F.; Ohanessian, G.; Clavaguéra, C. Dynamics of ions in a water drop using the AMOEBA polarizable force field. *Chem. Phys. Lett.* **2017**, *671*, 131–137.

(6) Asthagiri, D.; Pratt, L. R.; Ashbaugh, H. Absolute hydration free energies of ions, ion–water clusters, and quasichemical theory. *J. Chem. Physics* **2003**, *119*, 2702–2708.

(7) Caleman, C.; Hub, J. S.; van Maaren, P. J.; van der Spoel, D. Atomistic simulation of ion solvation in water explains surface preference of halides. *Proc. Natl. Acad. Sci. U.S.A.* **2011**, *108*, 6838–6842.

(8) Burnham, C. J.; Petersen, M. K.; Day, T. J.; Iyengar, S. S.; Voth, G. A. The properties of ion-water clusters. II. Solvation structures of Na+, Cl-, and H+ clusters as a function of temperature. *J. Chem. Phys.* **2006**, *124*, 024327.

(9) Petersen, M. K.; Iyengar, S. S.; Day, T. J.; Voth, G. A. The hydrated proton at the water liquid/vapor interface. *J. Phys. Chem. B* **2004**, *108*, 14804–14806.

(10) Hvelplund, P.; Kurten, T.; Støchkel, K.; Ryding, M. J.; Nielsen, S. B.; Uggerud, E. Stability and structure of protonated clusters of ammonia and water, H+ (NH3) m (H2O) n. *J. Phys. Chem. A* **2010**, *114*, 7301–7310.

(11) Fournier, J. A.; Wolke, C. T.; Johnson, M. A.; Odbadrakh, T. T.; Jordan, K. D.; Kathmann, S. M.; Xantheas, S. S. Snapshots of proton accommodation at a microscopic water surface: Understanding the vibrational spectral signatures of the charge defect in cryogenically cooled H+ (H2O) n= 2–28 clusters. *J. Phys. Chem. A* **2015**, *119*, 9425–9440.

(12) Gorlova, O.; DePalma, J. W.; Wolke, C. T.; Brathwaite, A.; Odbadrakh, T. T.; Jordan, K. D.; McCoy, A. B.; Johnson, M. A. Characterization of the primary hydration shell of the hydroxide ion with H2 tagging vibrational spectroscopy of the OH^--(H2O) n= 2, 3 and OD^--(D2O) n= 2, 3 clusters. *J. Chem. Phys.* **2016**, *145*, 134304.

(13) Consta, S. Fragmentation reactions of charged aqueous clusters. *J. Mol. Struct. THEOCHEM* **2002**, *591*, 131–140.

(14) Consta, S.; Mainer, K. R.; Novak, W. Fragmentation mechanisms of aqueous clusters charged with ions. *J. Chem. Phys.* **2003**, *119*, 10125–10132.

(15) Znamenskiy, V.; Marginean, I.; Vertes, A. Solvated ion evaporation from charged water nanodroplets. *J. Phys. Chem. A* **2003**, *107*, 7406–7412.

(16) Ahadi, E.; Konermann, L. Surface charge of electrosprayed water nanodroplets: A molecular dynamics study. *J. Am. Chem. Soc.* **2010**, *132*, 11270–11277.

(17) Malevanets, A.; Consta, S. Variation of droplet acidity during evaporation. *J. Chem. Phys.* **2013**, *138*, 184312.

(18) Consta, S. Manifestation of Rayleigh instability in droplets containing multiply charged macroions. *J. Phys. Chem. B* **2010**, *114*, 5263–5268.

(19) Sharawy, M.; Consta, S. Effect of counterions on the charging mechanisms of a macromolecule in aqueous nanodrops. *J. Chem. Phys.* **2014**, *141*, 104321.

(20) In Oh, M.; Paliy, M.; Consta, S. "Star" morphologies of charged nanodrops comprised of conformational isomers. *J. Chem. Phys.* **2018**, *148*, 024307.

(21) Sharawy, M.; Consta, S. Characterization of "star" droplet morphologies induced by charged macromolecules. *J. Phys. Chem. A* **2016**, *120*, 8871–8880.

(22) Miller, M. A.; Bonhommeau, D. A.; Moerland, C. P.; Gray, S. J.; Gaigeot, M.-P. Dynamics and thermodynamics of decay in charged clusters. *Mol. Phys.* **2015**, *113*, 2428–2434.

(23) Kaller, W.; Horvath, H. Charge and size distribution of medical aerosols. *Journal of Aerosol Science* **1996**, *27*, S399–S400.

(24) Malik, S. A.; Ng, W. H.; Bowen, J.; Tang, J.; Gomez, A.; Kenyon, A. J.; Day, R. M. Electrospray synthesis and properties of hierarchically structured PLGA TIPS microspheres for use as controlled release technologies. *J. Colloid Interface Sci.* **2016**, *467*, 220–229.

(25) Bain, R. M.; Pulliam, C. J.; Cooks, R. G. Accelerated Hantzsch electrospray synthesis with temporal control of reaction intermediates. *Chem. Sci.* **2015**, *6*, 397–401.

(26) Chen, X.; Cooks, R. G. Accelerated reactions in field desorption mass spectrometry. *J. Mass Spectrom.* **2018**, *53*, 942–946.

(27) Schrader, R. L.; Fedick, P. W.; Mehari, T. F.; Cooks, R. G. Accelerated chemical synthesis: Three ways of performing the Katritzky transamination reaction. *J. Chem. Educ.* **2019**,

(28) Lee, J. K.; Banerjee, S.; Nam, H. G.; Zare, R. N. Acceleration of reaction in charged microdroplets. *Q. Rev. Biophys.* **2015**, *48*, 437–444.

(29) Ingram, A. J.; Boeser, C. L.; Zare, R. N. Going beyond electrospray: mass spectrometric studies of chemical reactions in and on liquids. *Chem. Sci.* **2016**, *7*, 39–55.

(30) Wilm, M. Principles of electrospray ionization. *Mol. Cell. Proteomics* **2011**, *10*, M111–009407.

(31) Hirabayashi, A.; Sakairi, M.; Koizumi, H. Sonic spray ionization method for atmospheric pressure ionization mass spectrometry. *Anal. Chem.* **1994**, *66*, 4557–4559.

(32) Blakley, C.; Vestal, M. Thermospray interface for liquid chromatography/mass spectrometry. *Anal. Chem.* **1983**, *55*, 750–754.

(33) Sakairi, M.; Kambara, H. Atmospheric pressure spray ionization for liquid chromatography/mass spectrometry. *Anal. Chem.* **1989**, *61*, 1159–1164.

(34) Kambara, H. Sample introduction system for atmospheric pressure ionization mass spectrometry of nonvolatile compounds. *Anal. Chem.* **1982**, *54*, 143–146.

(35) Kebarle, P.; Verkerk, U. H. Electrospray: from ions in solution to ions in the gas phase, what we know now. *Mass Spectrom. Rev.* **2009**, *28*, 898–917.

(36) Dole, M.; Mack, L.; Hines, R.; Mobley, R.; Ferguson, L.; Alice, M. d. Molecular beams of macroions. *J. Chem. Phys.* **1968**, *49*, 2240–2249.

(37) Fenn, J. B. Ion formation from charged droplets: roles of geometry, energy, and

time. *J. Am. Soc. Mass. Spectrom.* **1993**, *4*, 524–535.

(38) Fenn, J. B.; Rosell, J.; Meng, C. K. In electrospray ionization, how much pull does an ion need to escape its droplet prison? *J. Am. Soc. Mass. Spectrom.* **1997**, *8*, 1147–1157.

(39) Mehmood, S.; Allison, T. M.; Robinson, C. V. Mass spectrometry of protein complexes: From origins to applications. *Annu. Rev. Phys. Chem.* **2015**, *66*, 453–474.

(40) Xia, Z.; Williams, E. R. Effect of droplet lifetime on where ions are formed in electrospray ionization. *Analyst* **2019**, *144*, 237–248.

(41) Rayleigh, L. XX. On the equilibrium of liquid conducting masses charged with electricity. *Philos. Mag.* **1882**, *14*, 184–186.

(42) Hendricks, C.; Schneider, J. Stability of a conducting droplet under the influence of surface tension and electrostatic forces. *Am. J. Phys* **1963**, *31*, 450–453.

(43) Peters, J. Rayleigh's electrified water drops. *Eur. J. Phys.* **1980**, *1*, 143.

(44) Consta, S.; Malevanets, A. Disintegration mechanisms of charged nanodroplets: novel systems for applying methods of activated processes. *Mol. Simul.* **2015**, *41*, 73–85.

(45) Oh, M. I.; Malevanets, A.; Paliy, M.; Frenkel, D.; Consta, S. When droplets become stars: charged dielectric droplets beyond the Rayleigh limit. *Soft Matter* **2017**, *13*, 8781–8795.

(46) Duft, D.; Lebius, H.; Huber, B. A.; Guet, C.; Leisner, T. Shape oscillations and stability of charged microdroplets. *Phys. Rev. Lett.* **2002**, *89*, 084503.

(47) Grimm, R. L.; Beauchamp, J. Evaporation and discharge dynamics of highly charged multicomponent droplets generated by electrospray ionization. *J. Phys. Chem. A* **2009**, *114*, 1411–1419.

(48) Varela, L. M.; Garcı??a, M.; Mosquera, V. Exact mean-field theory of ionic solutions: non-Debye screening. *Phys. Rep.* **2003**, *382*, 1–111.

(49) Israelachvili, J. The different faces of poly (ethylene glycol). *Proc. Natl. Acad. Sci. U.S.A.* **1997**, *94*, 8378–8379.

(50) Consta, S.; Chung, J. K. Charge-induced conformational changes of PEG-(Na(n)(+)) in a vacuum and aqueous nanodroplets. *J. Phys. Chem. B* **2011**, *115*, 10447–10455.

(51) Phillips, J. C.; Braun, R.; Wang, W.; Gumbart, J.; Tajkhorshid, E.; Villa, E.; Chipot, C.; Skeel, R. D.; Kalé, L.; Schulten, K. Scalable molecular dynamics with NAMD. *J. Comput. Chem.* **2005**, *26*, 1781–1802.

(52) Humphrey, W.; Dalke, A.; Schulten, K. VMD: Visual Molecular Dynamics. *J. Mol. Graphics* **1996**, *14*, 33–38.

(53) Vega, C.; de Miguel, E. Surface tension of the most popular models of water by using the test-area simulation method. *J. Chem. Phys.* **2007**, *126*, 154707.

(54) Zakharov, V. V.; Brodskaya, E. N.; Laaksonen, A. Surface properties of water clusters: a molecular dynamics study. *Mol. Phys.* **1998**, *95*, 203–209.

(55) Zakharov, V. V.; Brodskaya, E. N.; Laaksonen, A. Surface tension of water droplets: A molecular dynamics study of model and size dependencies. *J. Chem. Phys.* **1997**, *107*, 10675–10683.

(56) Jorgensen, W. L.; Jenson, C. Temperature dependence of TIP3P, SPC, and TIP4P water from NPT Monte Carlo simulations: Seeking temperatures of maximum density. *J. Comput. Chem.* **1998**, *19*, 1179–1186.

(57) Mahoney, M. W.; Jorgensen, W. L. A five-site model for liquid water and the reproduction of the density anomaly by rigid, nonpolarizable potential functions. *J. Chem. Phys.* **2000**, *112*, 8910–8922.

(58) Mark, P.; Nilsson, L. Structure and dynamics of the TIP3P, SPC, and SPC/E water models at 298 K. *J. Phys. Chem. A* **2001**, *105*, 9954–9960.

(59) Tolman, R. C. The effect of droplet size on surface tension. *J. Chem. Phys.* **1949**, *17*, 333–337.

(60) Homman, A.-A.; Bourasseau, E.; Stoltz, G.; Malfreyt, P.; Strafella, L.; Ghoufi, A. Surface tension of spherical drops from surface of tension. *J. Chem. Phys.* **2014**, *140*, 034110.

(61) Block, B. J.; Das, S. K.; Oettel, M.; Virnau, P.; Binder, K. Curvature dependence of surface free energy of liquid drops and bubbles: A simulation study. *J. Chem. Phys.* **2010**, *133*, 154702.

(62) Rowlinson, J. A drop of liquid. *J. Phys.: Condens. Matter* **1994**, *6*, A1.

(63) Horsch, M.; Hasse, H.; Shchekin, A. K.; Agarwal, A.; Eckelsbach, S.; Vrabec, J.; Müller, E. A.; Jackson, G. Excess equimolar radius of liquid drops. *Physical Review E* **2012**, *85*, 031605.

(64) Malijevskỳ, A.; Jackson, G. A perspective on the interfacial properties of nanoscopic liquid drops. *J. Phys.: Condens. Matter* **2012**, *24*, 464121.

(65) G Segovia-López, J.; Carbajal-Domínguez, A. Pressure tensor of nanoscopic liquid drops. *Entropy* **2015**, *17*, 1916–1935.

(66) Tröster, A.; Oettel, M.; Block, B.; Virnau, P.; Binder, K. Numerical approaches to determine the interface tension of curved interfaces from free energy calculations. *J. Chem. Phys.* **2012**, *136*, 064709.

(67) Jackson, J. D. *Classical Electrodynamics*, third ed. ed.; John Wiley & Sons: New York, NY, 1998.

(68) Atkins, K. Ions in liquid helium. *Phys. Rev.* **1959**, *116*, 1339.

(69) Leiderer, P.; Shikin, V. Applicability of the Atkins model to the ion behavior in superfluid helium. *J. Phys. Conf. Ser.* **2009**, *150*, 032048.

(70) Bartl, P.; Leidlmair, C.; Denifl, S.; Scheier, P.; Echt, O. On the size and structure of helium snowballs formed around charged atoms and clusters of noble gases. *J. Phys. Chem. A* **2013**, *118*, 8050–8059.

(71) Consta, S.; Malevanets, A. Manifestations of charge induced instability in droplets effected by charged macromolecules. *Phys. Rev. Lett.* **2012**, *109*, 148301.

(72) Szukalo, R. Interplay of hydrophobic/hydrophylic interactions in droplets. The University of Western Ontario, 2018; Undergraduate thesis.

(73) Consta, S.; Kapral, R. Dynamics of proton transfer in mesoscopic clusters. *J. Chem. Phys.* **1996**, *104*, 4581–4590.

(74) Consta, S.; Kapral, R. Proton transfer in mesoscopic, molecular clusters. *J. Chem. Phys.* **1994**, *101*, 10908–10914.

(75) Résibois, P. M. V. *Electrolyte theory*; Harper & Row, 1968.

(76) Ennis, J.; Marčelja, S.; Kjellander, R. Effective surface charge for symmetric electrolytes in the primitive model double layer. *Electrochim. Acta* **1996**, *41*, 2115–2124.

(77) Galassi, M.; Davies, J.; Theiler, J.; Gough, B.; Jungman, G.; Alken, P.; Booth, M.; Rossi, F. GNU scientific library. *Reference Manual edition* **2007**, *1*.

(78) Iribarne, J. V.; Thomson, B. A. On the evaporation of small ions from charged

droplets. *J. Chem. Phys.* **1976**, *64*, 2287–2294.

(79) Thomson, B.; Iribarne, J. Field induced ion evaporation from liquid surfaces at atmospheric pressure. *J. Chem. Phys.* **1979**, *71*, 4451–4463.

(80) Lebedev, V.; Laikov, D. A quadrature formula for the sphere of the 131st algebraic order of accuracy. *Doklady. Mathematics* **1999**, *59*, 477–481.

(81) R Core Team, R: A Language and Environment for Statistical Computing. R Foundation for Statistical Computing: Vienna, Austria, 2017.

(82) Soleilhac, A.; Dagany, X.; Dugourd, P.; Girod, M.; Antoine, R. Correlating droplet size with temperature changes in electrospray source by optical methods. *Anal. Chem.* **2015**, *87*, 8210–8217.

(83) Gibson, S. C.; Feigerle, C. S.; Cook, K. D. Fluorometric measurement and modeling of droplet temperature changes in an electrospray plume. *Anal. Chem.* **2013**, *86*, 464–472.

(84) Chung, J. K.; Consta, S. Release mechanisms of poly(ethylene glycol) macroions from aqueous charged nanodroplets. *J. Phys. Chem. B* **2012**, *116*, 5777–5785.

(85) Soltani, S.; Oh, M. I.; Consta, S. Effect of solvent on the charging mechanisms of poly (ethylene glycol) in droplets. *J. Chem. Phys.* **2015**, *142*, 114307.

(86) Oh, M. I.; Consta, S. Charging and release mechanisms of flexible macromolecules in droplets. *J. Am. Soc. Mass. Spectrom.* **2017**, *28*, 2262–2279.

(87) Yu, H.; Whitfield, T. W.; Harder, E.; Lamoureux, G.; Vorobyov, I.; Anisimov, V. M.; MacKerell Jr, A. D.; Roux, B. Simulating monovalent and divalent ions in aqueous solution using a Drude polarizable force field. *J. Chem. Theory Comput.* **2010**, *6*, 774–786.

(88) Spezia, R.; Migliorati, V.; D'Angelo, P. On the development of polarizable and Lennard-Jones force fields to study hydration structure and dynamics of actinide (III) ions based on effective ionic radii. *J. Chem. Phys.* **2017**, *147*, 161707.